THE JOURNAL OF BIOLOGICAL CHEMISTRY VOL. 287, NO. 21, pp. 17297–17307, May 18, 2012

Dual Role of the Molybdenum Cofactor Biosynthesis Protein MOCS3 in tRNA Thiolation and Molybdenum Cofactor Biosynthesis in Humans*

Received for publication, February 8, 2012, and in revised form, March 20, 2012 Published, JBC Papers in Press, March 27, 2012, DOI 10.1074/jbc.M112.351429

Mita Mullick Chowdhury[‡], **Carsten Dosche**[§1], **Hans-Gerd Löhmannsröben**[§], **and Silke Leimkühler**[‡2]

From the [‡]*Institute of Biochemistry and Biology, Department of Molecular Enzymology, and* [§]*Institute of Chemistry, Department of Physical Chemistry, University of Potsdam, Potsdam 14476, Germany*

Background: E1-like proteins are required for activation and thiocarboxylation of β-grasp fold proteins involved in sulfur transfer to cofactors and tRNA.
Results: MOCS3 interacts with both URM1 and MOCS2A *in vivo* and *in vitro*.
Conclusion: Molybdenum cofactor biosynthesis and tRNA thiolation steps are linked by the MOCS3 protein in humans.
Significance: The studies contribute to understanding the mechanism of protein conjugation and thiocarboxylate formation in sulfur transfer pathways.

We studied two pathways that involve the transfer of persulfide sulfur in humans, molybdenum cofactor biosynthesis and tRNA thiolation. Investigations using human cells showed that the two-domain protein MOCS3 is shared between both pathways. MOCS3 has an N-terminal adenylation domain and a C-terminal rhodanese-like domain. We showed that MOCS3 activates both MOCS2A and URM1 by adenylation and a subsequent sulfur transfer step for the formation of the thiocarboxylate group at the C terminus of each protein. MOCS2A and URM1 are β-grasp fold proteins that contain a highly conserved C-terminal double glycine motif. The role of the terminal glycine of MOCS2A and URM1 was examined for the interaction and the cellular localization with MOCS3. Deletion of the C-terminal glycine of either MOCS2A or URM1 resulted in a loss of interaction with MOCS3. Enhanced cyan fluorescent protein and enhanced yellow fluorescent protein fusions of the proteins were constructed, and the fluorescence resonance energy transfer efficiency was determined by the decrease in the donor lifetime. The cellular localization results showed that extension of the C terminus with an additional glycine of MOCS2A and URM1 altered the localization of MOCS3 from the cytosol to the nucleus.

Ubiquitin (Ub)[3] and ubiquitin-like proteins (Ubls) are involved in a large number of diverse processes within the eukaryotic cell. The regulation is achieved by the covalent conjugation of the Ubls to target proteins via a lysine residue. Only recently, it was discovered that Ubls are not restricted to eukaryotes, with the identification of Pup in bacteria (1) and the characterization of SAMP proteins in archaea (2, 3).

Ub-like protein conjugation is dependent on the activation of the C-terminal Gly-Gly motif in an ATP-dependent process, facilitating the formation of an acyl-adenylate and the subsequent thioester formation on a conserved cysteine residue of the activating enzyme (E1) and the Ubl. A cascade of enzymes (E2 and E3) is further involved in transesterification reactions for the transfer of the Ubl to a lysine residue of the target protein by formation of an isopeptide bond.

The E1-catalyzed activation of the Ubl resembles the second step of the molybdenum cofactor (Moco) biosynthesis in humans and bacteria. For Moco biosynthesis in humans, the E1-like protein MOCS3 forms a thiocarboxylate group at the C-terminal glycine of the β-grasp fold protein MOCS2A (4–6). Moco is required for the activity of xanthine dehydrogenase, aldehyde oxidase, sulfite oxidase, and the mitochondrial amidoxime reducing components, hmARC1 and hmARC2, in humans (7). In Moco, two sulfur atoms of the molybdopterin (MPT) moiety coordinate the molybdenum atom in the final structure (8). Therefore, incorporation of two sulfur atoms in the first intermediate of Moco biosynthesis, cyclic pyranopterin monophosphate (cPMP), is required. The sulfur is mobilized from L-cysteine by NFS1, a pyridoxal phosphate-dependent L-cysteine desulfurase, which forms a persulfide group on its conserved Cys-381 residue (9). The persulfide group is further transferred to Cys-412 of the C-terminal rhodanese-like domain (RLD) of MOCS3 (10, 11). The N-terminal MOCS3 domain shares amino acid homologies to ubiquitin-activating E1-like enzymes and to the *Escherichia coli* MoeB protein. In the activated MOCS3-MOCS2A acyl-adenylate complex, the sulfur from the C-terminal RLD is transferred to MOCS2A, forming a thiocarboxylate group at Gly-88 of MOCS2A and releasing MOCS3 and AMP (5). MOCS2A subsequently interacts with MOCS2B, which binds cPMP and generates MPT after the transfer of two sulfur atoms from two MOCS2A proteins (8). The major difference between the activation of Ub and

* This work was supported by Deutsche Forschungsgemeinschaft Grant LE1171/5-3 (to S. L.).
[1] Present address: Institute of Pure and Applied Chemistry, University of Oldenburg, 26111 Oldenburg, Germany.
[2] To whom correspondence should be addressed. Tel.: 49-331-977-5603; Fax: 49-331-977-5128; E-mail: sleim@uni-potsdam.de.
[3] The abbreviations used are: Ub, ubiquitin; Ubl, ubiquitin-like modifier; Moco, molybdenum cofactor; MPT, molybdopterin; cPMP, cyclic pyranopterin monophosphate; FRET, Förster resonance energy transfer; RLD, rhodanese-like domain; Ni-NTA, nickel nitrilotriacetate, RU, response unit; ECFP, enhanced cyan fluorescent protein; EYFP, enhanced yellow fluorescent protein; SPR, surface plasmon resonance.

the second step of the Moco biosynthesis is found in the underlying sulfur chemistry, because Ub activation involves thioester formation, and the thiocarboxylate formation is based on persulfide group transfer (12).

MOCS3 was shown to additionally interact with URM1, a ubiquitin-like modifier involved in the specific formation of 2-thiouridine tRNA in humans (5, 13, 14). In general, several modified nucleosides containing sulfur atoms were found in tRNA molecules, namely 2-thiocytidine (s^2C), 2-thiouridine (s^2U) derivatives, 4-thiouridine (s^4U), and 2-methylthioadenosine (ms^2A) (15). In particular, the 2-thio group of s^2U derivatives is known to ensure accurate deciphering of the genetic code and stabilization of the tRNA structure. So far, in eukaryotes the system in *Saccharomyces cerevisiae* is the best characterized. Here, the wobble bases of tRNAs contain two thiouridines, 5-methoxycarbonylmethyl-2-thiouridine ($mcm^5s^2U^{34}$) in cytoplasmic tRNAs and 5-carboxymethyl-2-thiouridine ($cmnm^5s^2U^{34}$) in mitochondrial tRNAs (16, 17).

S. cerevisiae Urm1 was identified as the component of a new protein conjugation system by Furukawa *et al.* (18). Here, Urm1 conjugates to Ahp1p (alkyl hydroperoxide reductase), a protein involved in oxidative stress tolerance (19). Urm1 has some unique features because it has a dual function in protein conjugation and as a sulfur carrier (20); its structure resembles more those of sulfur carriers, like ThiS (21) and MoaD (22), which are involved in the biosynthesis of sulfur-containing cofactors, like Moco and thiamin, and therefore it presents a link between ubiquitin conjugation systems and the evolutionary older cofactor biosynthesis (23).

Only recently has it been shown that urmylation also occurs in humans and is involved in oxygen stress tolerance (23). It was shown that human URM1 is conjugated to lysine residues of target proteins in its own pathway and that oxidative stress enhances protein urmylation in mammalian cells. However, mechanisms underlying the dual function in protein conjugation and sulfur transfer are still controversially discussed, because on the one hand in cofactor biosynthesis persulfide formation is essential and on the other hand thioester formation is needed for Ub conjugation (12, 23). Therefore, the mechanism of both conjugation and thiocarboxylation by Ubls has to be further elucidated. For such a purpose, URM1 displays an excellent example because it is combining both functions. As sulfur carrier, we proposed that MOCS3 connects the two distinct processes in the cell, for Moco biosynthesis and tRNA thiolation, especially because it is the only E1-like activating enzyme that is present in humans for these pathways (5).

In this study, we show that MOCS3 interacts with both URM1 and MOCS2A in human cells. We analyzed the cellular localization of the proteins in addition to their interaction by fluorescence resonance energy transfer (FRET). The FRET efficiency was calculated by determination of the decrease in the donor lifetime. Because the Gly-Gly motif is the one common sequence feature of the Ubls involved in both acyl adenylation and thioester or acyl-disulfide formation, the role of the terminal glycine was examined in MOCS2A and URM1, and the effects of the variations on both pathways were compared. In addition, we examined the importance of the C-terminal Gly-Gly motif in terms of its role for the localization of the proteins.

EXPERIMENTAL PROCEDURES

Bacterial Strains, Media, and Growth Conditions—Cell strains containing expression plasmids were grown aerobically at 30 °C in LB medium containing 150 μg/ml ampicillin or 50 μg/ml chloramphenicol.

E. coli MoaE was expressed in BL21(DE3) cells from plasmid pMWaE15 and purified as described previously by Wuebbens and Rajagopalan (24). Human MOCS2A and URM1 wild type proteins were expressed and purified as described previously by Schmitz *et al.* (5).

Site-directed Mutagenesis, Protein Expression, and Purification—Single amino acid substitutions at the C termini of the human URM1 or MOCS2A proteins were created using PCR mutagenesis, resulting in URM1-G101A, URM1-G101Δ, and URM1–102G+ or MOCS2A-G88A, MOCS2A-G88Δ, and MOCS2A-89G+ variants, respectively. For expression of the variants, the URM1 cDNA was cloned into the pACYC-duet 1 BglII restriction site, and the MOCS2A cDNA was cloned into the sites NdeI and KpnI of pTYB2. *E. coli* BL21(DE3) cells and ER2566 were used for heterologous expression of URM1 and MOCS2A variants, respectively, as described previously (5).

Expression of MOCS3—Sf9 insect cells, derived from *Spodoptera frugiperda* (Invitrogen), were grown as suspension culture in Sf-900-II SFM medium (Invitrogen) supplemented with 2% fetal bovine serum (FBS, PAN-Biotech, Germany) at 28 °C and 180 rpm. For infection with recombinant baculovirus, cells were grown as monolayer cultured at 28 °C in a humidified incubator.

The restriction sites BamHI and XbaI were introduced into the MOCS3 cDNA by PCR, which allowed cloning into the pFastBacI vector (Bac-to-Bac baculovirus expression system, Invitrogen). The resulting plasmid was designated pMMC30 and expressed MOCS3 as an N-terminal fusion to a His_6 tag. Positive recombinant bacmids were used to transfect Sf9 cells using Cellfectin II (Invitrogen) and to produce a baculovirus stock. For protein expression Sf9 cells were infected with high titer viral stock (P2). Cells were harvested by centrifugation 72 h after infection and lysed by sonification, and the supernatant was subjected to Ni-NTA chromatography. MOCS3-RLD was expressed and purified as described previously (5, 10).

Cell Culture Techniques—HeLa and HEK 293 cells were cultured in Dulbecco's modified Eagle's medium (DMEM, PAN-Biotech, Germany) supplemented with 10% FBS (PAN-Biotech, Germany). Cell cultures were maintained at a temperature of 37 °C and 5% CO_2 atmosphere.

Construction of ECFP and EYFP Fusion Proteins—Enhanced cyan fluorescence protein (ECFP) and enhanced yellow fluorescence protein (EYFP) are among the most used FRET pairs (25). Because the donor fluorescence of ECFP is comparably dim, and sensitized emission of the acceptor is hard to detect due to the spectral bleed through of ECFP fluorescence, therefore the fluorescence lifetime of the donor was chosen as parameter to monitor FRET.

MOCS3 cDNA was amplified by PCR and cloned into pECFP-C1 (Clontech) vector using BamHI and SalI restriction sites, resulting in plasmid pZM13. MOCS2A and URM1 variants were cloned using SacI and HindIII restriction sites and

ligated as N-terminal fusion proteins into pEYFP-C1 (Clontech) resulting in pMMC2 and pMMC4, respectively.

MPT Synthase Reactions—MPT synthase reactions were performed at room temperature in a total volume of 400 μl of 100 mM Tris-HCl (pH 7.2). The produced MPT was converted to the stable oxidation product Form A and quantified as described by the published procedures (26, 27). The reaction mixtures contained 5 μM of *E. coli* MoaE, 5 μM MOCS3, 2.5 mM Mg-ATP, 0.6 mM Na_2S or sodium thiosulfate, and 15 μM of each MOCS2A variant. The reaction was initiated by the addition of 2.5 μM cPMP, which was purified as described previously (28).

Thiosulfate Sulfurtransferase Activity of MOCS3—The sulfurtransferase activity of MOCS3 was measured according to the procedure described by Sörbo (29) in 100 mM Hepes (pH 8.0). For determination of the K_m and k_{cat} values, each reaction contained 130 nM MOCS3, 5–500 mM sodium thiosulfate, and 0.1–50 mM potassium cyanide in a total volume of 500 μl. Thiocyanate was quantified as iron complex by its absorption at 460 nm ($\epsilon = 4200\ M^{-1}cm^{-1}$).

MOCS3-catalyzed Adenylation of MOCS2A and URM1 Variants—For adenylation of MOCS2A and URM1 variants by MOCS3, 20 μM of each protein pair was incubated at 25 °C with 250 μM Mg-ATP, and 2 units of inorganic pyrophosphatase in a total volume of 300 μl. After 90 min, the reaction was stopped by addition of 1% SDS and additional heat inactivation at 95 °C for 15 min. To obtain protein-free extracts, samples were transferred to Amicon Ultra concentrators (molecular mass cutoff of 10 kDa, Millipore) and centrifuged at 10,000 × *g* for 15 min. The flow-through was collected, and AMP was quantified using the published procedure (27).

In Vitro tRNA Synthesis—For quantification of tRNA thiolation by the URM1 variants, the specific tRNA for lysine (UUU) was synthesized *in vitro*. For synthesis, the following primers were used $tRNA^{Lys(UUU)}$Fw: 5′-TAATACGACTCACTATAGCCCGGATAGCTCAGTCGGTAGAGCATCAGACTTTTAATCTG-3′ and $tRNA^{Lys(UUU)}$Rev: 5′-CGCCCGAACAGGGACTTGAACCCTGGACCCTCAGATTAAAAGTCT-3′. Primers were annealed, and single-stranded DNA was synthesized by a reverse transcriptase reaction using the RevertAid™ H minus kit (Fermentas). Single-stranded DNA was purified using the Extract II kit (Macherey & Nagel) which served as a template for *in vitro* transcription using T7 RNA polymerase. Synthesized tRNA was separated by urea containing PAGE. Gel bands corresponding to tRNA were excised, and tRNA was dissolved in buffer and concentrated by ethanol precipitation.

In Vitro tRNA Thiolation and Nucleoside Analysis—To quantify the ability of URM1 and the variants to transfer sulfur to the wobble uridine of $tRNA^{Lys(UUU)}$, we incubated 200 μg of $tRNA^{Lys(UUU)}$, 5 μM MOCS3, 10 μM URM1, 2.5 mM Mg-ATP, and 1 mM sodium sulfide. In addition, 10 μM CTU2 was included in the reaction, which was expressed in *E. coli* with an N-terminal His_6 tag and purified by Ni-NTA chromatography and subsequent size exclusion chromatography. The reaction was carried out in a total volume of 200 μl and incubated for 60 min at RT. Afterward, the thiolated tRNA was precipitated with ethanol and resuspended in 200 μl of 50 mM sodium acetate (pH 5.3) and 20 mM zinc acetate. 3 units of nuclease P1 was added, and the mixture was incubated overnight at 37 °C. Subsequently, 10 μl of 1 M Tris and 4 units of FastAP (Fermentas) were added, and the mixture was incubated for an additional 16 h at 37 °C. Nucleoside analysis was performed as described by Gehrke *et al.* (30) using a LiChrospher 100 RP 18 column (5 μm, 250 × 4.6 mm).

Surface Plasmon Resonance (SPR) Measurements—All bindings experiments were conducted on an SPR-based Biacore™T200 instrument on CM5 sensor chips at a temperature of 25 °C and a flow of 30 μl/min using the control T200 software and evaluation T200 software (GE Healthcare). The autosampler rack containing the samples was cooled throughout the entire measurements to 8 °C. Immobilization of proteins yield the following response units (RU) per flow cell: BSA, 698 RU; MOCS3 787 RU. As running buffer, 20 mM phosphate, 150 mM NaCl, 0.005% (v/v) Tween 20 (pH 7.4) was used. URM1 and MOCS2A variants with concentrations of 0.16, 0.31, 0.63, 1.25, 2.5, 5, 10, and 20 μM were injected for 4.5 min at a flow rate of 30 μl/min followed by a 15-min dissociation using the kinject command and regeneration of the sensor surface with 50 mM HCl for 1 min. As a control, BSA was used as ligand. Binding curves were corrected by subtraction of buffer injection curves for both flow cells.

Cellular Localization Studies and FRET Analysis—HEK293 or HeLa cells were grown on poly-L-lysine-coated coverslips. Transient transfection of the cells was performed using a modified calcium phosphate method. The DNA/calcium mixture was added dropwise to the cells, and the medium was replaced with fresh culture medium after 8 h. 16–20 h after transfection, cells were fixed for 30 min using 4% paraformaldehyde in PBS at 4 °C. The cells were washed twice with PBS and mounted onto slides with Mowiol (Roth). Images for subcellular localization were conducted at a Zeiss LSM710 (Zeiss, Jena, Germany) laser scanning confocal microscope equipped with a PlanApo 1.4/63× objective.

For fluorescence lifetime imaging microscopy, a Visitron Systems imaging system based on an inverted microscope (Axio Observer, Zeiss) equipped with an Infinity 3 confocal scanning head and an additional total internal reflection port were used. As excitation light source, a mode locked ps Nd-YAG laser with regenerative amplifier (PL2201/TH, Ekspla) was used. The third harmonic output at 355 nm and a repetition rate of 1 kHz was 30 μJ/pulse. The output of the Nd-YAG laser was coupled free space without collimation optics into a 500-μm quartz fiber bundle. This fiber bundle was connected to the total internal reflection port at the rear side of the microscope via a 355-nm dichroic mirror. Inside the microscope, an arrangement consisting of an additional 355-nm dichroic filter and a 400-nm cutoff filter was used for the separation of excitation and fluorescence emission light. To spectrally separate the ECFP and EYFP emissions, a dual view module (MAG Biosystems) was placed between microscope and detector. This module was equipped with a dichroic filter set for 485 and 540 nm, respectively, with a 30-nm bandpass for each channel.

For time-gated detection, an iCCD camera (Pimax2, Princeton Instruments) was used. For all measurements, 100 frames with a time increment of 0.25 and 1.8 ns gate width were acquired to monitor an overall time interval of 25 ns. For each single frame, 250 pulses were integrated on a chip. To synchro-

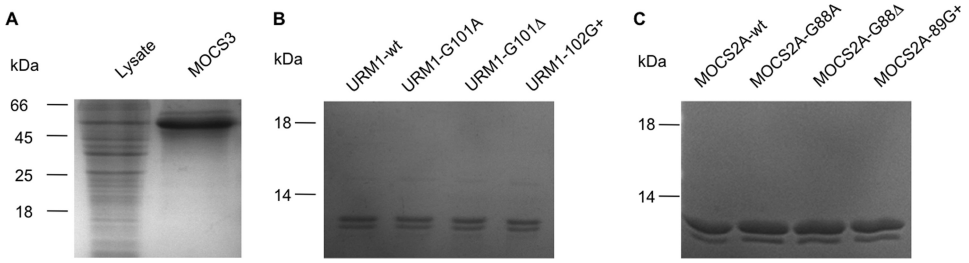

FIGURE 1. **Purification of MOCS3, MOCS2A, URM1 and their variants.** *A,* purification of MOCS3. 4 μg of MOCS3 was separated by 15% SDS-PAGE and stained with Coomassie Brilliant Blue. *B,* purification of URM1; *C,* purification of MOCS2A. After purification, 3 μg each of wild type protein and the indicated variants were separated on a 15% SDS-polyacrylamide gel and stained with Coomassie Brilliant Blue.

nize the iCCD camera to the laser, the Q-switch monitor output of the laser was used to trigger the TTL input of the CCD control unit. Confocal images were acquired with a CoolSnap HQ^2 CCD camera (Photometrics) attached to the Infinity 3 confocal scanning head. Samples were excited with an Ar-Kr ion laser (Innova C70, Coherent) at 456 nm for ECFP or 514 nm for EYFP. Data acquisition and processing were performed with the Metamorph 7.2 software (Molecular Devices). At least 40 cells for each sample were measured. The efficiency of FRET was determined by measuring the donor lifetime of ECFP alone (τ_D) and in the presence of an acceptor (τ_{DA}).

RESULTS

Expression and Purification of Human MOCS3 from Sf9 Cells—Earlier attempts to purify the holo-MOCS3 protein in an active form failed after expression in heterologous systems like *E. coli*, *Pichia pastoris,* or *S. cerevisiae*. Here, an approach was chosen to express human MOCS3 in a baculovirus insect cell system in Sf9 cells. The *MOCS3* gene was cloned into the pFastBac1 vector resulting in a fusion of the expressed recombinant protein with an N-terminal His_6 tag. The Sf9 cells were grown as suspension cultures transfected at a density of 1×10^6 cells/ml with recombinant virus and harvested by centrifugation 72 h post-infection. The soluble fraction of the cell lysate containing MOCS3 was purified by Ni-NTA chromatography. After elution, one major band was detected on Coomassie Brilliant Blue R stained SDS-polyacrylamide gels with a size of ~52 kDa (Fig. 1*A*), corresponding to the calculated molecular mass of 56,695 Da for His_6-tagged MOCS3. The protein was purified with a yield of 1.4 mg/100 ml of Sf9 cells and a purity of more than 90%.

Analysis of the Thiosulfate:Sulfur Transfer Activity of MOCS3—Previous studies using the single C-terminal rhodanese-like domain of MOCS3 (MOCS3-RLD) demonstrated that in an *in vitro* reaction the protein transfers sulfur from thiosulfate to cyanide (10). The sulfur is bound as a persulfide on Cys-412 of the MOCS3-RLD, the first residue of the conserved six-amino acid active site loop characteristic for rhodaneses (10, 31). Here, we compared the thiosulfate sulfurtransferase activity of holo-MOCS3 purified from Sf9 cells to the activity of its separately purified RLD expressed in *E. coli* cells. The kinetic constants are listed in Table 1 and show that holo-MOCS3 and MOCS3-RLD have comparable k_{cat} and K_m values, showing that MOCS3 was purified with a functional C-terminal RLD from Sf9 cells. The low catalytic efficiency with thiosulfate as sulfur source shows that thiosulfate is likely not the physiological substrate of MOCS3, as already described by Krepinsky and Leimkühler (31) in a study using the MOCS3-RLD protein. *In vivo*, the sulfur donor for MOCS3 was proposed to be the L-cysteine desulfurase NFS1 (11), a protein also involved in FeS cluster biogenesis.

TABLE 1
Kinetic parameters of holo-MOCS3 and MOCS3-RLD with thiosulfate as sulfur source

Apparent k_{cat} and K_m values were determined using the assay described by Sörbo (29) with 5–500 mM sodium thiosulfate and 0.1–50 mM potassium cyanide.

	k_{cat}	$K_m^{thiosulfate}$	$K_m^{cyanide}$
	s^{-1}	mM	mM
MOCS3	2.11 ± 0.20	80.8 ± 3.8	0.50 ± 0.09
MOCS3-RLD	1.85 ± 0.18	98.5 ± 4.5	0.67 ± 0.11

Site-directed Mutagenesis of MOCS2A and URM1—The amino acid sequence comparison of URM1 and MOCS2A showed an identity of 24%, with the most striking feature being the C-terminal double glycine motif (Fig. 2). To compare the role of the C-terminal Gly-Gly motif of MOCS2A and URM1 for the interaction with MOCS3, the following single amino acid variants were generated and purified: URM1: G101A, G101Δ, and 102G+; MOCS2A: G88A, G88Δ, and 89G+.

The proteins were expressed in a heterologous expression system in *E. coli* and purified by ammonium sulfate precipitation and size exclusion chromatography (URM1) or by chitin affinity chromatography (MOCS2A). All variants exhibited expression and purification characteristics similar to those of the wild type proteins, showing that the amino acid changes did not cause significant structural changes that result in protein instability or altered solubility (Fig. 1, *B* and *C*). The proteins were purified with a yield of ~3 mg/liter of expression culture and a purity of at least 95%. For both URM1 and MOCS2A, two bands were obtained after purification (Fig. 1, *B* and *C*). By MS/MS peptide mapping, we determined that both bands corresponded to URM1 or MOCS2A, respectively, most likely reflecting the presence of the adenylated and nonadenylated species as shown before for *E. coli* MoaD (32).

Analysis of the MOCS3-catalyzed Adenylation of MOCS2A and URM1 Variants—The first step of activation of both MOCS2A and URM1 consists of the formation of an acyl-adenylate group at the C-terminal glycine residue. To test the activity of the N-terminal MoeB-like domain of purified MOCS3, the adenylation efficiency of MOCS3 was analyzed with MOCS2A and URM1 wild type in addition to the generated protein variants. The incubation mixtures contained MOCS3, Mg-ATP, inorganic pyrophosphatase, and either MOCS2A or URM1 variants. The reaction was stopped after

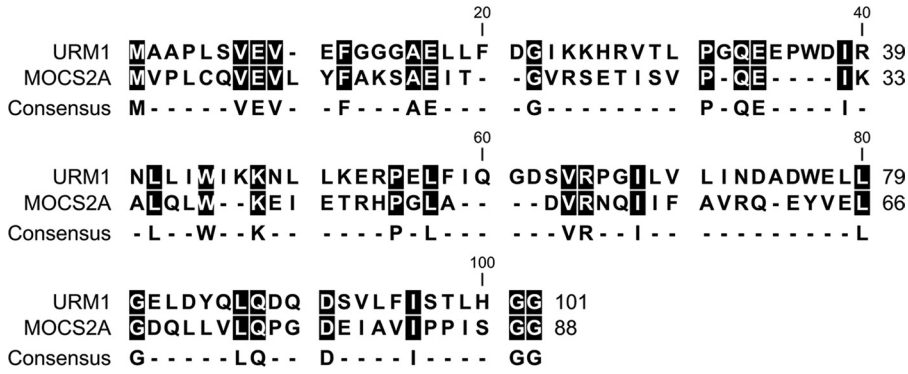

FIGURE 2. **Amino acid sequence alignment of human MOCS2A and human URM1.** Identical amino acids are shaded in *black*.

varying time points by the addition of 1% SDS and a heat inactivation step. The released AMP was separated on an HPLC reversed phase column and detected by its absorption at 260 nm. A maximum rate of AMP production (1 mol of AMP/mol of protein) was obtained after 90 min for the wild type proteins. The results in Fig. 3 show that the C-terminal glycine is essential for the adenylation of both MOCS2A and URM1, because a deletion of the last glycine resulted in a complete loss of AMP formation. The variation of the last glycine of both of URM1 and MOCS2A resulted in reduced AMP levels. However, the effect in MOCS2A-G88A was more pronounced with 67% reduction in AMP production in comparison with Urm1-G101A, where the level was only 23% reduced. When an additional glycine was added, the adenylation efficiency in URM1 was reduced to 40% and in MOCS2A to 23%. Overall, the amino acid variations had the same effect on the adenylation efficiency of both proteins, and in MOCS2A, only the amino acid exchanges had a higher impact on the overall reaction.

Analysis of the Rate of MPT Formation by MOCS2A—After formation of the acyl-adenylate on the C terminus of MOCS2A, sulfur is transferred from the C-terminal MOCS3-RLD, and a thiocarboxylate group is formed. In case of MOCS2A, two thiocarboxylated proteins then transfer the sulfur to MOCS2B-bound cPMP, and MPT is released. To determine whether the alterations at the C terminus of MOCS2A affected MPT formation, a defined *in vitro* system was used consisting of purified cPMP, MOCS3, *E. coli* MoaE, Mg-ATP, inorganic pyrophosphatase, and MOCS2A. We substituted MOCS2B by *E. coli* MoaE in our assay, which was shown to be more active *in vitro* (8). As sulfur source, either sodium sulfide or thiosulfate were used. Sulfide can be added to activated MOCS2A-AMP without the activity of the C-terminal RLD of MOCS3, whereas thiosulfate is converted to sulfite and a protein-bound persulfide on MOCS3-RLD, which is then transferred further on to MOCS2A. Like this, the activity of the RLD can be determined and compared with the direct sulfur transfer with sulfide *in vitro*. For quantification, produced MPT was converted to its stable oxidation product Form A by oxidation with acidic iodine. The reaction mixtures were separated on a reversed-phase HPLC column, and Form A was quantified by its fluorescence. As shown in Fig. 4 (*white bars*), when sulfide was used as sulfur source, the effect on MPT production of the MOCS2A variants correlated to the adenylation efficiency shown above. The MOCS2A-G88Δ variant showed a level of 5% MPT produced in the assay in comparison with wild type MOCS2A. When using the MOCS2A-89G+ and MOCS2A-G88A variants, the MPT levels were reduced to 39 or 59%, respectively. When thiosulfate was used as a sulfur source, the results obtained were comparable (Fig. 4, *black bars*); however, the overall reaction was less effective and showed a reduction of

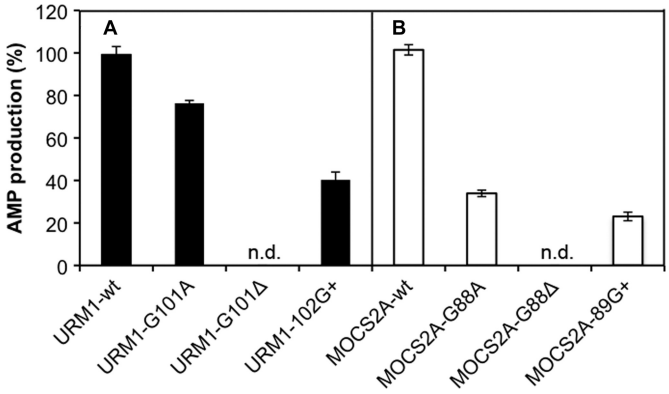

FIGURE 3. **AMP production by MOCS3.** Reaction mixtures contained 20 μM of each URM1 variant (*A*) or 20 μM of each MOCS2A variant (*B*), 250 μM Mg-ATP, 2 units of inorganic pyrophosphatase, and 20 μM MOCS3. The reactions were stopped by addition of 1% SDS, and for complete release of AMP, the samples were additionally incubated for 15 min at 95 °C. *n.d.,* not detectable.

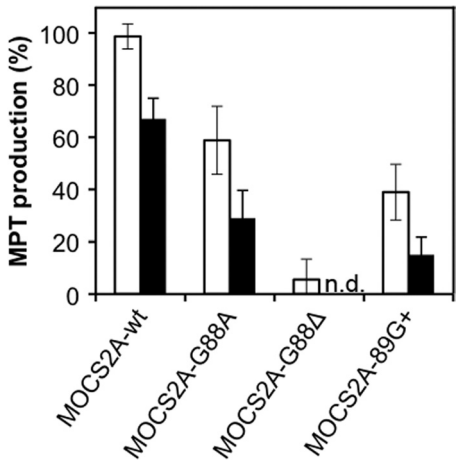

FIGURE 4. **MPT production by MOCS2A and its variants.** MPT was produced using an *in vitro* system consisting of 5 μM MOCS3, 5 μM MoaE, 1.4 μM cPMP, and 15 μM MOCS2A with either sulfide (*white bars*) or thiosulfate (*black bars*) as sulfur source. Reaction mixtures were incubated for 90 min at room temperature and after oxidation of MPT, Form A was quantified by fluorescence detection on a reversed phase HPLC C18 column. For each MOCS2A variant, three independent measurements were performed. *n.d.,* not detectable.

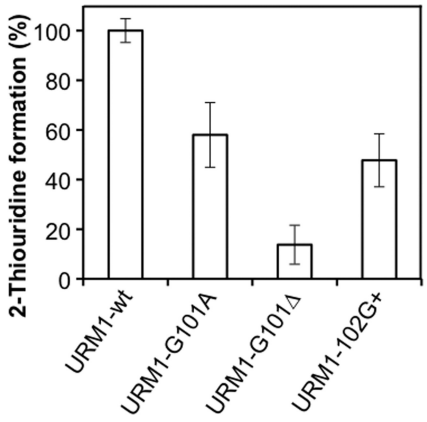

FIGURE 5. **2-Thiouridine formation by URM1 and its variants.** 2-Thiouridine formation was determined using an *in vitro* system consisting of 10 μM CTU2, 5 μM MOCS3, 200 microgram μg of synthesized $tRNA^{Lys(UUU)}$, 1 mM sodium sulfide, 2.5 mM Mg-ATP, and 10 μM of each URM1 variant. Reaction mixtures were incubated 60 min at RT, and nucleosides were separated by HPLC after precipitation and digestion of tRNAs.

MPT production of 25% under the assay conditions. This might imply that only 75% of the purified MOCS3 has an active RLD. In total, the results are highly consistent with the adenylation level of the MOCS2A variants and show that thiocarboxylate formation and adenylation of MOCS2A correlate.

Quantification of tRNA Thiolation Efficiency by URM1—URM1 transfers the sulfur of the thiocarboxylate group to the wobble uridine 34 of tRNAs, namely $tRNA^{Lys\ (UUU)}$, $tRNA^{Gln\ (UUG)}$, and $tRNA^{Glu\ (UUC)}$. The introduction of sulfur at the 2-position results in the formation of s^2U or mcm^5s^2U. Prior to the sulfuration reaction, the uridine is proposed to be activated in an ATP-dependent manner by the CTU1-CTU2 complex (33). It was shown previously (16) that in a defined *in vitro* system using isolated $tRNA^{Lys(UUU)}$, URM1, Uba4, and Ncs6 and the yeast homologues of MOCS3 and CTU1, 2-thiouridine was readily formed. The tRNA was digested; nucleosides were separated, and formed thionucleosides were quantified. Using this procedure, we analyzed the effects of the alterations of the Gly-Gly motif of URM1 on the rate of 2-thiouridine formation. The results shown in Fig. 5 reveal that a drastic reduction of s^2U was observed for the URM1-G101Δ variant, whereas for the URM1-G101A and URM1–102G+ variants, s^2U was detected at a level of 58 and 48%, respectively, in comparison with wild type URM1 (Fig. 5). The results are highly consistent with the adenylation level of the URM1 variants and show that thiocarboxylate formation and adenylation of URM1 correlate.

Analysis of Protein-Protein Interactions by Surface Plasmon Resonance Measurements—To analyze the influence on the C-terminal glycine of MOCS2A and URM1 on the interaction and complex formation with MOCS3 *in vitro*, SPR measurements were employed for real time detection of the specific interactions using the purified proteins.

Only in the presence of 100 μM ATP in the running buffer was an interaction of MOCS3 with the wild type MOCS2A or URM1 proteins determined. K_D values of 0.26 μM for URM1-MOCS3 and 0.47 μM for MOCS2A-MOCS3 were determined using a 1:1 binding model. In case of URM1-G101A, binding curves were monitored; however, because the response did not correspond to a 1:1 binding model, a K_D value could not be calculated. For the other variants, no apparent interactions with the immobilized MOCS3 were detectable. The results show that the effects of the variation of the C-terminal glycine of MOCS2A and URM1 variants observed above are based on an impaired ability of the proteins to form a stable complex with MOCS3. SPR was unable to resolve the differences in the interaction between MOCS3 and alteration of the C terminus of MOCS2A and URM1, which were detected in the activity assays. Additionally, the results show that the interaction of MOCS2A or URM1 with MOCS3 is more stable in the presence of ATP, as reported before for the Ub-E1 interaction (34).

Analysis of the Effects of MOCS2A and URM1 Variants on Their Cellular Localization and the Interaction with MOCS3 in Human Cells—To further investigate the role of the C-terminal glycine of MOCS2A and URM1 *in vivo*, the variants were expressed as an N-terminal EYFP fusion in HeLa cells. As reported previously (10), our investigations determined that MOCS3 was located in the cytoplasm, whereas MOCS2A showed a dual localization in the cytoplasm and the nucleus (Fig. 6*A*). URM1 showed a similar distribution like MOCS2A, with a localization in the nucleus and in the cytoplasm of HeLa and HEK293 cells (Fig. 6*B*, data not shown). In the localization studies, we identified a correlation between the length of the Gly-Gly motif and the subcellular localization of the two proteins. When the C-terminal glycine of URM1 was deleted, the overexpressed protein was solely identified in the cytosol (Fig. 6*B*). In addition, the MOCS2A-G88Δ variant showed lower levels of fluorescence within the nucleus compared with the cytoplasm, which likely corresponds to lower levels in protein amount (Fig. 6*A*). A similar pattern was observed for the expression of MOCS2A-G88A (Fig. 6*A*). In case of the extension of the Gly-Gly motif by one residue, both Ubls exhibited expression like the wild type proteins, with a localization both in the cytosol and the nucleus. Surprisingly, when MOCS3 was co-expressed with MOCS2A-89G+ or URM1–101G+, MOCS3 was additionally located in the nucleus (Fig. 6*B*), revealing an influence not only on the localization of the Ubls themselves but also in addition to the activating enzyme.

Furthermore, we also determined the cellular *in vivo* interaction of MOCS3 with either MOCS2A or URM1 by analyzing their fluorescence resonance energy transfer (FRET). Either N-terminally tagged ECFP or EYFP variants were used, and the FRET efficiency was calculated by determining the decrease in the ECFP donor lifetime. The lifetime was determined by fluorescence lifetime imaging microscopy measurements with an excitation of ECFP at 355 nm and the decay curves were measured in an overall time interval of 25 ns. The decay curves were fitted bi-exponentially with a long lifetime component of $\tau_1 = \tau_D = 3.9 \pm 0.1$ ns and a short lifetime of $\tau_2 = 1.2 \pm 0.1$ ns in the shorter range, which corresponds to an internal conformational change in ECFP as reported before (35). As positive control, a protein fusion of ECFP and EYFP with peptide linker was used, for which the donor long lifetime component was reduced to $\tau_1 = \tau_{DA} = 2.8 \pm 0.1$ ns, although the short lifetime of $\tau_2 = 1.2 \pm 0.1$ ns remained constant (Fig. 7). This corresponds to a decrease in the lifetime of 26%. In comparison, the co-expression of ECFP and EYFP alone without the peptide linker did not alter the donor lifetime (Fig. 7). The FRET resulting from the

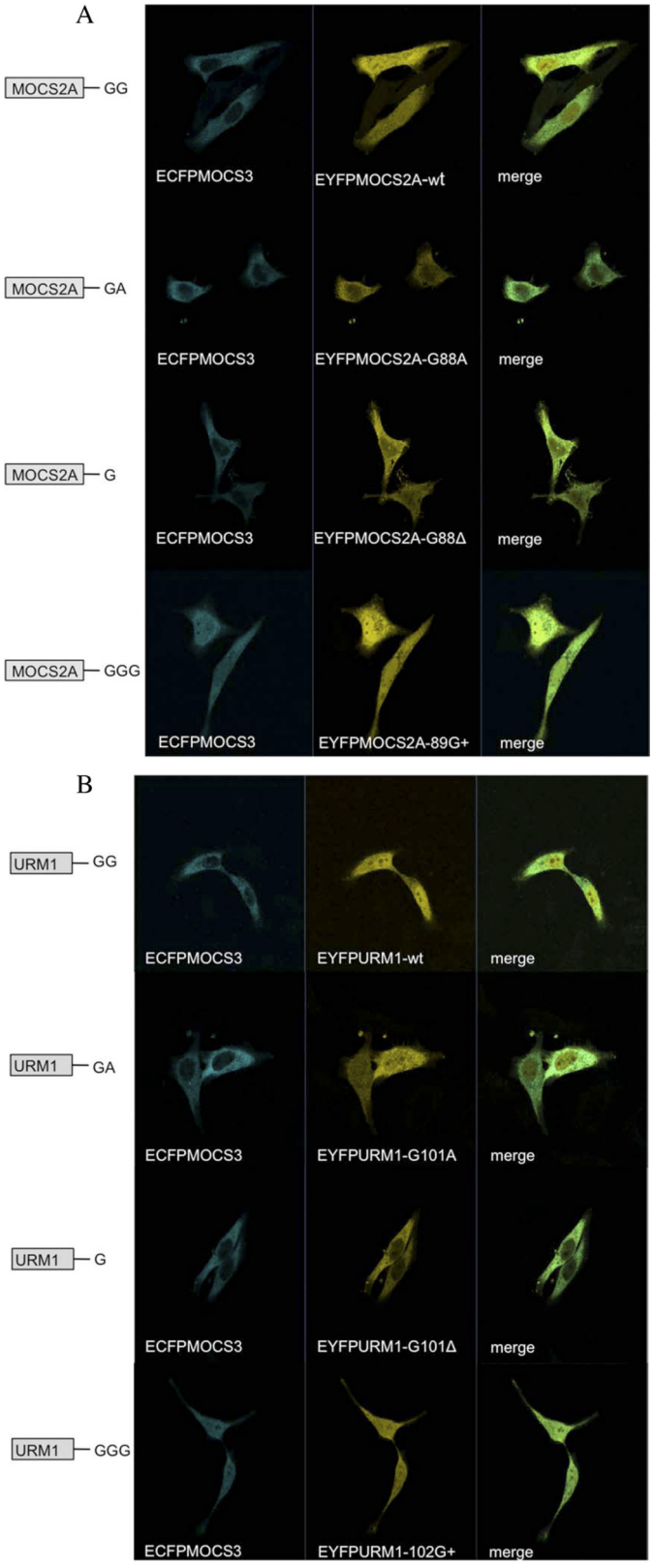

FIGURE 6. **Localization of MOCS3, MOCS2A, and URM1 in HeLa cells.** *A,* co-localization of ECFP-MOCS3 and EYFP-tagged URM1 variants in HeLa cells. *B,* co-localization of ECFP-MOCS3 and EYFP-MOCS2A variants in HeLa cells. HeLa cells were co-transfected with plasmids encoding an N-terminal ECFP-MOCS3 fusion protein and N-terminal tagged EYFP-URM1 or EYFP-MOCS2A. Cells were fixed 24 h post-transfection. Localization of MOCS3 and URM1 or MOCS2A variants were determined by confocal microscopy using LSM 710 and the ZEN software for linear unmixing of the two dyes.

co-expression of MOCS3 with wild type MOCS2A and URM1 resulted in a reduction of 20% in the donor lifetime, due to a higher distance between the fluorophores in the heteromeric complex compared with the distance in the ECFP-EYFP fusion protein. When EYFP was fused to the C terminus of either URM1 or MOCS2A, the ECFP-MOCS3 fusion did not change its lifetime, showing that the proteins were unable to interact due to the C-terminal EYFP location.

The resulting lifetimes of the N-terminal EYFP-MOCS2A and URM1 fusions with ECFP-MOCS3 are shown in Fig. 7. The results show that replacement of the ultimate glycine of URM1 by alanine resulted in a minor decrease in donor lifetime, whereas deletion or addition of a glycine to URM1 resulted in a drastic decrease in the donor lifetime (Fig. 7*B*). Thus, the proteins were not able to efficiently interact *in vivo*.

In case of MOCS2A, the alteration of the ultimate glycine in the MOCS2A-G88A variant resulted in reduced FRET efficiencies, whereas the deletion of the ultimate residue in MOCS2A-G88Δ abolished the energy transfer from ECFP completely (Fig. 7*C*). In contrast, in MOCS2A-89G+, the addition of a C-terminal glycine resulted in a decrease in lifetime that was not as pronounced as for the URM1–102G+ variant. In total, the results are highly consistent with the obtained activities for the protein variants and show that the interaction of both proteins is primarily determined by the C-terminal glycine of the β-grasp fold protein.

DISCUSSION

In this report, we expressed and purified MOCS3 in a baculovirus insect cell system from Sf9 cells, which so far is the only suitable system for the expression of MOCS3. All other attempts to express MOCS3 in eukaryotic systems like *P. pastoris* or *S. cerevisiae* did not yield an active enzyme. Thus, for the first time we were able to demonstrate that MOCS3 was purified in an active form from Sf9 cells, and we demonstrated that both the N-terminal E1/MoeB-like domain and the C-terminal RLD are active. The first indications that MOCS3 might interact with both URM1 and MOCS2A were obtained from *in vitro* studies in which MOCS3 was replaced by the *S. cerevisiae* homologue Uba4 (5). The *in vitro* interaction studies showed that Uba4 was able to interact with both human MOCS2A and human URM1. In addition to the interaction, in these studies we were able to demonstrate that a thiocarboxylate group is formed on URM1 *in vitro*. Later, the thiocarboxylate on Urm1 was confirmed by *in vivo* studies (23). Even though *S. cerevisiae* harbors both URM1-mediated tRNA thiolation and its protein conjugation to Ahp1p, it is not an ideal model system, because the genes for Moco biosynthesis, including MOCS2A are absent in this organism. Thus, *S. cerevisiae* is not a suitable model organism to prove a shared pathway for Moco biosynthesis and tRNA thiolation.

To investigate the role of MOCS3 as a partner for both MOCS2A and URM1 in human cells, we performed FRET studies and investigated the donor lifetime as an indication for the strength of the interaction of the protein pairs. MOCS3 and either MOCS2A or URM1 were co-expressed as ECFP/EYFP fusion proteins in HeLa cells to determine the FRET between the fluorescent dyes. Because of the high dependence of the

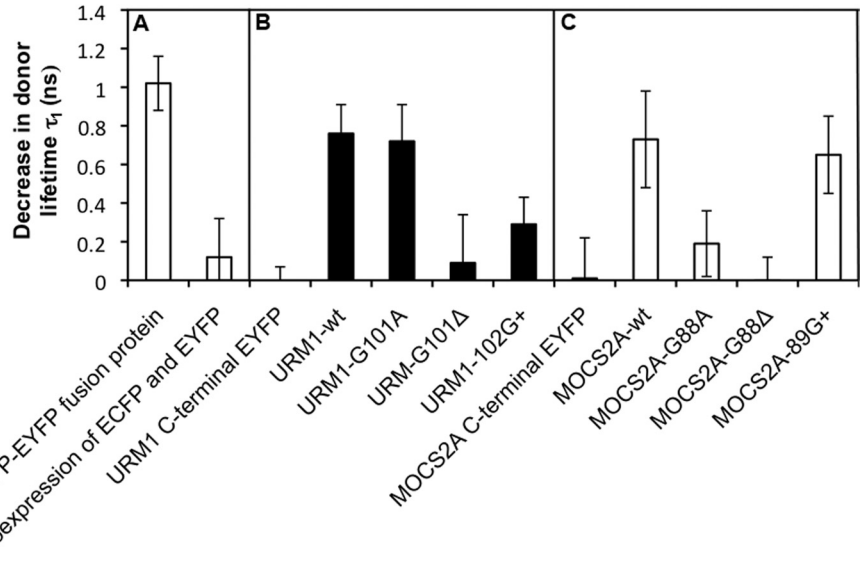

FIGURE 7. **Quantification of the decrease in donor lifetime.** FRET was determined in HeLa cells after expression of ECFP- and EYFP-tagged proteins by donor lifetime measurement. *A,* as controls, co-expression of ECFP and EYFP and an ECFP-EYFP fusion protein was tested. The decrease in donor lifetime of the ECFP-MOCS3 fusion protein in the presence of EYFP-tagged variants of URM1 (*B*) and MOCS2A (*C*) is shown. For each value at least 40 cells were measured.

distance between the dyes, only the complex formation between MOCS3 and the candidates enable an energy transfer. Our results obtained from the donor lifetime measurements showed that MOCS3 is able to interact with both MOCS2A and URM1 in HeLa cells. The same results were additionally obtained in HEK 293 cells (data not shown). Because a similar decay in donor lifetime was obtained, this also revealed a similar distance between the proteins, reflecting similar interaction sites.

For the activation reaction, MOCS3 has to form a heterotetrameric complex with URM1 or MOCS2A, as described previously for Uba4 (5) or the *E. coli* congeners MoaD and MoeB (4). The crystal structure of the *E. coli* $(MoaD\text{-}MoeB)_2$ complex showed that it is composed of a central MoeB dimer with a MoaD subunit at each end of the dimer. The C terminus (residues 76–81) is extended into the pocket on the MoeB surface (4) and is therefore accessible for activation. The yeast Urm1 crystal structure is very similar to the MoaD structure that has two additional α-helices, as compared with other Ubls (20), and thus it is more similar to MoaD in this respect. The structure of yeast Urm1 revealed a hydrophobic patch on the surface that is similar to MoaD, and because this region is exposed it might be essential for interaction with MOCS3 (20). Overall, URM1 and MOCS2A share an amino acid sequence identity of 24% (Fig. 2). The double glycine motif at their C termini is the only striking feature in both proteins. To investigate the role of the C-terminal glycine for both proteins for the interaction with MOCS3 in addition to their reactivity, several amino acid variations at the C-terminal glycine were generated. The main purpose was to identify differences between both proteins, because URM1 is a dual function protein and acts in protein conjugation and as a sulfur carrier, and the role of MOCS2A is restricted to act as a sulfur carrier in Moco biosynthesis.

The C-terminal glycine is involved in the first activation step of MOCS2A or URM1 that is catalyzed by MOCS3, involving the formation of an acyl-adenylate as an essential prerequisite for subsequent formation of the thiocarboxylate (5). Our results show that the alteration of the terminal glycine motif had the same effects on URM1 and MOCS2A, because all variants showed an impaired rate of adenylation. In addition, also the variation of the length of the glycine motif had similar effects in both Ubls. The deletion of the C-terminal residue totally abolished adenylation, whereas the extension of the motif by one glycine solely reduced the efficiency of the acyl-adenylate formation. The glycine to alanine exchange of the ultimate glycine of URM1 resulted in a slightly impaired ability to form an acyl-adenylate; in contrast, the adenylation efficiency for MOCS2A was diminished to about a third compared with the wild type protein.

Considering that the formation of the acyl-adenylate is only the first step of the ATP-dependent activation catalyzed by MOCS3, which is followed by the subsequent thiocarboxylation catalyzed by the RLD, we investigated the sulfur transfer reaction of thiocarboxylated MOCS2A to cPMP. In our studies, MOCS3 was able to thiocarboxylate MOCS2A and the variants using either sulfide or thiosulfate, showing that both domains of MOCS3 are at least 75% active (31). To determine the sulfur transfer rate, MPT formation was monitored. The results showed comparable values as obtained for the rate of adenylation of the proteins, with the MOCS2A-G88Δ variant having the most prominent effect (23). Similarly, we investigated the transfer of sulfur to the wobble uridine of the $tRNA^{Lys(UUU)}$ by URM1 and the variants. In an *in vitro* system consisting of MOCS3, CTU2, Mg-ATP, and sodium sulfide, URM1 was able to catalyze 2-thiouridine formation. The exchange of the C-terminal glycine to alanine and the addition of a glycine decreased the rate of 2-thiouridine formation to 50%, although the deletion of the last glycine had a more severe impact showing only 10% of thiouridine. These results are in good agreement to the findings of van der Veen *et al.* (23) where no thiocarboxylation of URM1-G101Δ could be detected *in vivo*, leading to an increase in hypomodified tRNA. Similar findings were also

obtained by Noma *et al.* (15) using the yeast Urm1-ΔGG variant, illustrating that deletion of both glycines had similar effects in comparison with the deletion of only the last glycine.

All effects of the variation of the Gly-Gly motif are based on insufficient complex formation with MOCS3, as shown *in vitro* by SPR measurements. For the wild type proteins in presence of ATP, K_D values in the nanomolar range were obtained. In comparison for the variants, only the URM1-G101A showed an impaired ability to form a complex, which did not obey a 1:1 binding and therefore did not allow the determination of a K_D value. The FRET studies revealed comparable effects *in vivo* that could be quantified, showing only a slightly impaired donor lifetime decrease for the variants compared with the more profound effects in case of the wild type proteins.

Our results are also in good agreement with a previous study investigating the role of the glycine motif of *E. coli* MoaD (27). These studies together underline the assumption that the ultimate glycine is optimized for the sulfur carrier role for Moco biosynthesis and tRNA thiolation and that especially the length of the tail of the Ubl is critical, because deletion of the tail generally resulted in a inactive protein for all Ubls (27). In contrast, the ubiquitin-G76A variant exhibited quantitatively acyl-adenylate and thioester formation with its E1 (36), which is consistent with our findings for the URM1-G101A variant, which also showed significant activities in acyl-adenylate formation. This implies that URM1 is more similar to the protein conjugation systems than MOCS2A, which is optimized to serve only as a sulfur carrier protein.

Surprisingly, while determining the FRET efficiency of URM1 and MOCS2A with MOCS3, an influence on the localization by the different variations was observed, revealing a connection between the alteration of the Gly-Gly motif and the subcellular localization. Generally, MOCS3 has a cytosolic localization, although URM1 and MOCS2A are both found in the cytosol and the nucleus. The different modifications at the C terminus of the Ubl affected the protein localization to the same extent, revealing a restricted localization to the cytosol for MOCS2A-G88A, MOCS2A-G88Δ, and URM1-G101Δ. In addition, the co-expression of MOCS3 with the variants of URM1 and MOCS2A with the C-terminal elongation of the Gly-Gly motif by one glycine showed not only a nuclear localization, like observed for the wild type proteins, but also an influence on the localization of their E1 partner, MOCS3, which exhibited an additional localization inside the nucleus. So far, it is unclear whether URM1 or MOCS2A has a specific role in the nucleus.

Very recently van der Veen *et al.* (23) identified targets of urmylation in humans, among which were parts of the tRNA thiolation machinery (CTU1 and CTU2) and a deubiquitinating enzyme (USP15), proteins involved in nuclear transport like CAS, and a protein involved in the shuttling between cytosol and nucleus. Taking into account that upon urmylation CAS was relocalized to the cytosol and the previous description of the influence of Ubl conjugation on the subcellular localization of proteins (23), there might be an effect on the localization of MOCS3 by its substrates.

Van der Veen *et al.* (23) additionally described the role of the nucleocytoplasmic shuttling factor CAS as a target of urmylation linking the nuclear transport to oxidative stress, which is in good agreement with the observation that nuclear import is haltered upon oxidant treatment as also reported by Kodiha *et al.* (37). Speculation on the influence of urmylation on the arrest of nuclear transport is underlined by similar phenotypes of CAS depletion (38) and URM1 silencing (13), which both result in the arrest in G_2/M phase.

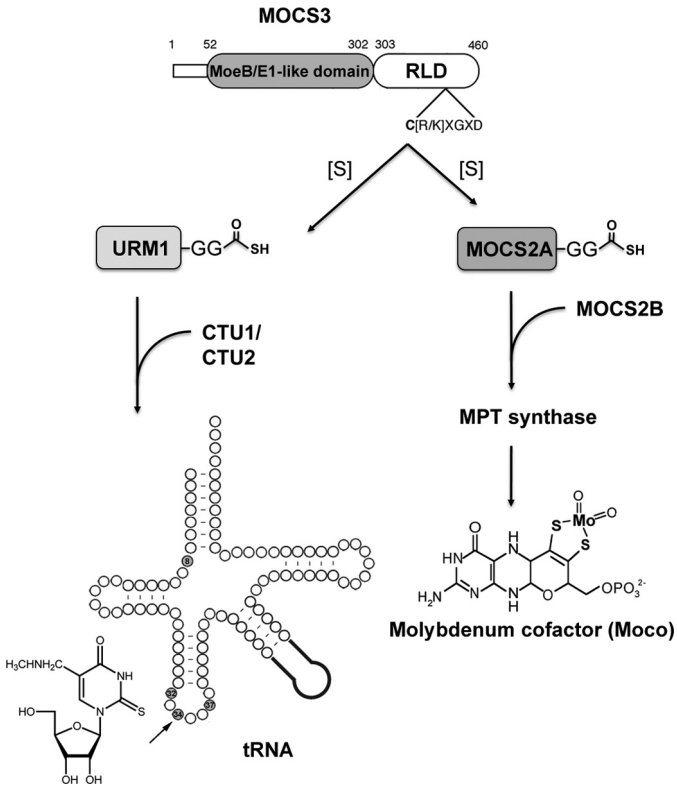

FIGURE 8. **Model for the interaction of MOCS3 with MOCS2A and URM1 in humans.** MOCS3 has an N-terminal MoeB/E1-like domain that adenylates MOCS2A and URM1. The C-terminal rhodanese-like domain (*RLD*) subsequently forms a thiocarboxylate on both proteins by sulfur transfer. URM1 transfers the sulfur group to uridine 34 on tRNA with the help of the proteins CTU1 and CTU2. MOCS2A forms the active MPT synthase with MOCS2B and transfers the sulfur for the formation of molybdopterin (*MPT*) in Moco biosynthesis.

However, the morphological abnormalities caused by reduction of cellular URM1 levels in HeLa cells by shRNA, which were shown to be increased cell size and the presence of multiple nuclei within a single cell, likely also result from translational errors, because the 2-thio modification is implicated in translational fidelity and efficacy as stated by Ikeuchi *et al.* (39). Additionally, similar findings were also reported for MOCS3 depletion in *Caenorhabditis elegans* (40). Here, depletion of the MOCS3 homologue reduced the levels of tRNA thiolation leading to misreading of an opal stop codon and subsequently the suppression of a multivulva phenotype, demonstrating the role of tRNA modification on global cellular processes in this organism. Furthermore, multinuclear cells were also observed after overexpression of URM1 in human cell cultures. These findings demonstrate an additional role of URM1 for cytokinesis and cell cycle progression. Taken together with the results presented herein, a contribution of URM1/MOCS3 to the control of global processes like nuclear transport, cytokinesis, and cell cycle progression is possible.

In comparison, yeast MDY2, a Ubl domain protein with no exposed C-terminal Gly-Gly motif, is associated to microtubule-directed nuclear migration, which might have additionally a potential role in these pathways, because MOCS3 was localized in centrosomes where the microtubule emanated. For MDY2, it was described that it is mostly localized in the nucleus, but upon heat stress the protein is relocalized to cytosolic granules. In MYD2, there is no evidence for C-terminal processing, but it is involved in nuclear migration via the microtubules, which emanates from spindle pole body, the yeast equivalent of the centrosome (41). For SUMO, it has been described that it is required for the recruitment of RanGAP1 to kinetochores and the mitotic spindle to control processes during mitosis (42), and it has an essential role in the control of nuclear protein import (43). Thus, MOCS3 might be shuttled into the nucleus by either URM1 or MOCS2A. However, whether MOCS3 has a role in the nucleus still has to be investigated.

Our data clearly show that MOCS3 marks the intersection of two pathways, tRNA thiolation and Moco biosynthesis, by activating both URM1 and MOCS2A in human cells (Fig. 8). Thus, MOCS3 might be the central switch to determine the faith of the persulfide sulfur at its C-terminal RLD. Because MOCS3 was also shown to be a target for urmylation (23), this might have a regulatory role on the activity of MOCS3 and its interaction with either URM1 or MOCS2A. The influence of urmylation on enzyme activity has to be investigated in future studies.

Acknowledgments—We thank Jennifer Schmitz for cloning the MOCS2A variants and help with the insect cells. We thank Zvonimir Marelja for cloning plasmid pZM13. Otto Baumann and Ralf Gräf (University of Potsdam) are thanked for help with confocal microscopy. The ECFP-EYFP fusion plasmid was provided by Sebastian Bandholtz (Charite). We are grateful to the Zoya Ignatova group (University of Potsdam) for assistance in tRNA preparation and Angelika Lehmann for performing the SPR experiments.

REFERENCES

1. Striebel, F., Imkamp, F., Sutter, M., Steiner, M., Mamedov, A., and Weber-Ban, E. (2009) Bacterial ubiquitin-like modifier Pup is deamidated and conjugated to substrates by distinct but homologous enzymes. *Nat. Struct. Mol. Biol.* **16,** 647–651
2. Humbard, M. A., Miranda, H. V., Lim, J. M., Krause, D. J., Pritz, J. R., Zhou, G., Chen, S., Wells, L., and Maupin-Furlow, J. A. (2010) Ubiquitin-like small archaeal modifier proteins (SAMPs) in *Haloferax volcanii*. *Nature* **463,** 54–60
3. Miranda, H. V., Nembhard, N., Su, D., Hepowit, N., Krause, D. J., Pritz, J. R., Phillips, C., Söll, D., and Maupin-Furlow, J. A. (2011) E1- and ubiquitin-like proteins provide a direct link between protein conjugation and sulfur transfer in archaea. *Proc. Natl. Acad. Sci. U.S.A.* **108,** 4417–4422
4. Lake, M. W., Wuebbens, M. M., Rajagopalan, K. V., and Schindelin, H. (2001) Mechanism of ubiquitin activation revealed by the structure of a bacterial MoeB-MoaD complex. *Nature* **414,** 325–329
5. Schmitz, J., Chowdhury, M. M., Hänzelmann, P., Nimtz, M., Lee, E. Y., Schindelin, H., and Leimkühler, S. (2008) The sulfur transferase activity of Uba4 presents a link between ubiquitin-like protein conjugation and activation of sulfur carrier proteins. *Biochemistry* **47,** 6479–6489
6. Schindelin, H. (2005) in *Protein Degradation 1. Ubiquitin and the Chemistry of Life* (Mayer, J. R., Ciechanover, A., Rechsteiner, M., eds) Vol. 1, pp. 21–43, Wiley-VCH Verlag, Weinheim, Germany
7. Hille, R., Nishino, T., and Bittner, F. (2011) Molybdenum enzymes in higher organisms. *Coord. Chem. Rev.* **255,** 1179–1205
8. Leimkuhler, S., Freuer, A., Araujo, J. A., Rajagopalan, K. V., and Mendel, R. R. (2003) Mechanistic studies of human molybdopterin synthase reaction and characterization of mutants identified in group B patients of molybdenum cofactor deficiency. *J. Biol. Chem.* **278,** 26127–26134
9. Mühlenhoff, U., Balk, J., Richhardt, N., Kaiser, J. T., Sipos, K., Kispal, G., and Lill, R. (2004) Functional characterization of the eukaryotic cysteine desulfurase Nfs1p from *Saccharomyces cerevisiae*. *J. Biol. Chem.* **279,** 36906–36915
10. Matthies, A., Rajagopalan, K. V., Mendel, R. R., and Leimkühler, S. (2004) Evidence for the physiological role of a rhodanese-like protein for the biosynthesis of the molybdenum cofactor in humans. *Proc. Natl. Acad. Sci. U.S.A.* **101,** 5946–5951
11. Marelja, Z., Stöcklein, W., Nimtz, M., and Leimkühler, S. (2008) A novel role for human Nfs1 in the cytoplasm. Nfs1 acts as a sulfur donor for MOCS3, a protein involved in molybdenum cofactor biosynthesis. *J. Biol. Chem.* **283,** 25178–25185
12. Petroski, M. D., Salvesen, G. S., and Wolf, D. A. (2011) Urm1 couples sulfur transfer to ubiquitin-like protein function in oxidative stress. *Proc. Natl. Acad. Sci. U.S.A.* **108,** 1749–1750
13. Schlieker, C. D., Van der Veen, A. G., Damon, J. R., Spooner, E., and Ploegh, H. L. (2008) A functional proteomics approach links the ubiquitin-related modifier Urm1 to a tRNA modification pathway. *Proc. Natl. Acad. Sci. U.S.A.* **105,** 18255–18260
14. Leidel, S., Pedrioli, P. G., Bucher, T., Brost, R., Costanzo, M., Schmidt, A., Aebersold, R., Boone, C., Hofmann, K., and Peter, M. (2009) Ubiquitin-related modifier Urm1 acts as a sulfur carrier in thiolation of eukaryotic transfer RNA. *Nature* **458,** 228–232
15. Noma, A., Shigi, N., and Suzuki, T. (2009) in *DNA and RNA Modification Enzymes: Structure, Mechanism, Function, and Evolution* (Grosjean, H., ed) pp. 392–405, Landes Bioscience, Austin, TX
16. Noma, A., Sakaguchi, Y., and Suzuki, T. (2009) Mechanistic characterization of the sulfur-relay system for eukaryotic 2-thiouridine biogenesis at tRNA wobble positions. *Nucleic Acids Res.* **37,** 1335–1352
17. Nakai, Y., Nakai, M., Lill, R., Suzuki, T., and Hayashi, H. (2007) Thio modification of yeast cytosolic tRNA is an iron-sulfur protein-dependent pathway. *Mol. Cell. Biol.* **27,** 2841–2847
18. Furukawa, K., Mizushima, N., Noda, T., and Ohsumi, Y. (2000) A protein conjugation system in yeast with homology to biosynthetic enzyme reaction of prokaryotes. *J. Biol. Chem.* **275,** 7462–7465
19. Goehring, A. S., Rivers, D. M., and Sprague, G. F., Jr. (2003) Attachment of the ubiquitin-related protein Urm1p to the antioxidant protein Ahp1p. *Eukaryot. Cell* **2,** 930–936
20. Xu, J., Zhang, J., Wang, L., Zhou, J., Huang, H., Wu, J., Zhong, Y., and Shi, Y. (2006) Solution structure of Urm1 and its implications for the origin of protein modifiers. *Proc. Natl. Acad. Sci. U.S.A.* **103,** 11625–11630
21. Lehmann, C., Begley, T. P., and Ealick, S. E. (2006) Structure of the *Escherichia coli* ThiS-ThiF complex, a key component of the sulfur transfer system in thiamin biosynthesis. *Biochemistry* **45,** 11–19
22. Rudolph, M. J., Wuebbens, M. M., Rajagopalan, K. V., and Schindelin, H. (2001) Crystal structure of molybdopterin synthase and its evolutionary relationship to ubiquitin activation. *Nat. Struct. Biol.* **8,** 42–46
23. Van der Veen, A. G., Schorpp, K., Schlieker, C., Buti, L., Damon, J. R., Spooner, E., Ploegh, H. L., and Jentsch, S. (2011) Role of the ubiquitin-like protein Urm1 as a noncanonical lysine-directed protein modifier. *Proc. Natl. Acad. Sci. U.S.A.* **108,** 1763–1770
24. Wuebbens, M. M., and Rajagopalan, K. V. (2003) Mechanistic and mutational studies of *Escherichia coli* molybdopterin synthase clarify the final step of molybdopterin biosynthesis. *J. Biol. Chem.* **278,** 14523–14532
25. Dardalhon, V., Noraz, N., Pollok, K., Rebouissou, C., Boyer, M., Bakker, A. Q., Spits, H., and Taylor, N. (1999) Green fluorescent protein as a selectable marker of fibronectin-facilitated retroviral gene transfer in primary human T lymphocytes. *Hum. Gene Ther.* **10,** 5–14
26. Johnson, J. L., Hainline, B. E., Rajagopalan, K. V., and Arison, B. H. (1984) The pterin component of the molybdenum cofactor. Structural characterization of two fluorescent derivatives. *J. Biol. Chem.* **259,** 5414–5422
27. Schmitz, J., Wuebbens, M. M., Rajagopalan, K. V., and Leimkühler, S.

(2007) Role of the C-terminal Gly-Gly motif of *Escherichia coli* MoaD, a molybdenum cofactor biosynthesis protein with a ubiquitin fold. *Biochemistry* **46,** 909–916
28. Wuebbens, M. M., and Rajagopalan, K. V. (1995) Investigation of the early steps of molybdopterin biosynthesis in *Escherichia coli* through the use of *in vivo* labeling studies. *J. Biol. Chem.* **270,** 1082–1087
29. Sörbo, B. (1957) A colorimetric method for the determination of thiosulfate. *Biochim. Biophys. Acta* **23,** 412–416
30. Gehrke, C. W., Kuo, K. C., McCune, R. A., and Gerhardt, K. (1982) Quantitative enzymatic hydrolysis of tRNAs. Reversed-phase high performance liquid chromatography of tRNA nucleosides. *J. Chromatogr.* **230,** 297–308
31. Krepinsky, K., and Leimkühler, S. (2007) Site-directed mutagenesis of the active site loop of the rhodanese-like domain of the human molybdopterin synthase sulfurase MOCS3. Major differences in substrate specificity between eukaryotic and bacterial homologs. *FEBS J.* **274,** 2778–2787
32. Leimkühler, S., Wuebbens, M. M., and Rajagopalan, K. V. (2001) Characterization of *Escherichia coli* MoeB and its involvement in the activation of molybdopterin synthase for the biosynthesis of the molybdenum cofactor. *J. Biol. Chem.* **276,** 34695–34701
33. Dewez, M., Bauer, F., Dieu, M., Raes, M., Vandenhaute, J., and Hermand, D. (2008) The conserved Wobble uridine tRNA thiolase Ctu1-Ctu2 is required to maintain genome integrity. *Proc. Natl. Acad. Sci. U.S.A.* **105,** 5459–5464
34. Ciechanover, A., Elias, S., Heller, H., and Hershko, A. (1982) "Covalent affinity" purification of ubiquitin-activating enzyme. *J. Biol. Chem.* **257,** 2537–2542
35. Rizzo, M. A., Springer, G. H., Granada, B., and Piston, D. W. (2004) An improved cyan fluorescent protein variant useful for FRET. *Nat. Biotechnol.* **22,** 445–449
36. Pickart, C. M., Kasperek, E. M., Beal, R., and Kim, A. (1994) Substrate properties of site-specific mutant ubiquitin protein (G76A) reveal unexpected mechanistic features of ubiquitin-activating enzyme (E1). *J. Biol. Chem.* **269,** 7115–7123
37. Kodiha, M., Tran, D., Morogan, A., Qian, C., and Stochaj, U. (2009) Dissecting the signaling events that impact classical nuclear import and target nuclear transport factors. *PLoS One* **4,** e8420
38. Ogryzko, V. V., Brinkmann, E., Howard, B. H., Pastan, I., and Brinkmann, U. (1997) Antisense inhibition of CAS, the human homologue of the yeast chromosome segregation gene CSE1, interferes with mitosis in HeLa cells. *Biochemistry* **36,** 9493–9500
39. Ikeuchi, Y., Shigi, N., Kato, J., Nishimura, A., and Suzuki, T. (2006) Mechanistic insights into sulfur relay by multiple sulfur mediators involved in thiouridine biosynthesis at tRNA wobble positions. *Mol. Cell* **21,** 97–108
40. Kim, S., Johnson, W., Chen, C., Sewell, A. K., Byström, A. S., and Han, M. (2010) Allele-specific suppressors of lin-1(R175Opal) identify functions of MOC-3 and DPH-3 in tRNA modification complexes in *Caenorhabditis elegans*. *Genetics* **185,** 1235–1247
41. Cohnen, A., Bielig, H., Hollenberg, C. P., Hu, Z., and Ramezani-Rad, M. (2010) The yeast ubiquitin-like domain protein Mdy2 is required for microtubule-directed nuclear migration and localizes to cytoplasmic granules in response to heat stress. *Cytoskeleton* **67,** 635–649
42. Joseph, J., Tan, S. H., Karpova, T. S., McNally, J. G., and Dasso, M. (2002) SUMO-1 targets RanGAP1 to kinetochores and mitotic spindles. *J. Cell Biol.* **156,** 595–602
43. Pichler, A., Gast, A., Seeler, J. S., Dejean, A., and Melchior, F. (2002) The nucleoporin RanBP2 has SUMO1 E3 ligase activity. *Cell* **108,** 109–120